

# Estimating Atmospheric Motion Winds from Satellite Image Data using Space-time Drift Models

Indranil Sahoo<sup>1</sup>, Joseph Guinness<sup>2</sup>, and Brian J. Reich<sup>3</sup>

<sup>1</sup>Department of Statistical Sciences and Operations Research,  
Virginia Commonwealth University

<sup>2</sup>Department of Statistics and Data Science, Cornell University

<sup>3</sup>Department of Statistics, North Carolina State University

## Abstract

Geostationary satellites collect high-resolution weather data comprising a series of images which can be used to estimate wind speed and direction at different altitudes. The Derived Motion Winds (DMW) Algorithm is commonly used to process these data and estimate atmospheric winds by tracking features in images taken by the GOES-R series of the NOAA geostationary meteorological satellites. However, the wind estimates from the DMW Algorithm are sparse and do not come with uncertainty measures. This motivates us to statistically model wind motions as a spatial process drifting in time. We propose a covariance function that depends on spatial and temporal lags and a drift parameter to capture the wind speed and wind direction. We estimate the parameters by local maximum likelihood. Our method allows us to compute standard errors of the estimates, enabling spatial smoothing of the estimates using a Gaussian kernel weighted by the inverses of the estimated variances. We conduct extensive simulation studies to determine the situations where our method performs well. The proposed method is applied to the GOES-15 brightness temperature data over Colorado and reduces prediction error of brightness temperature compared to the DMW Algorithm.

*Keywords:* Derived Motion Winds, Asymmetry, Spatio-temporal processes, Maximum likelihood estimation, Spatial smoothing, GOES-15

# 1 Introduction

Winds are an important component of atmospheric circulation, and estimating local or regional winds is particularly important for making weather forecasts. They influence vegetation as they affect factors that influence plant growth, such as seed dispersal rates, air transportation of pollen, and metabolism rates in plants. The study of local winds also permits evaluation of power produced by wind turbines (Brown et al. 1984, Castino et al. 1998), prediction of propagation of oil-spills (Kim et al. 2014) and the study of coastal erosion (Ahmad et al. 2015). Local winds are capable of moving pollutants into an area. For example, Calima, which blows dust into the Canary Islands (WeatherOnline 2018). Winds may also impact large-scale devastation such as forest fires. For example, the Santa Ana winds which blow into California after scorching summers (Berkowitz & Steckelberg 2017). Thus it is important to map the strength and direction of local winds to help us prepare for natural calamities and facilitate preventive measures.

Observations of wind speed and direction at the ground level are collected at weather stations on land and by buoys or ships over oceans. Low orbit satellites such as Jason 3 and Sentinel 1 infer surface winds using geophysical inversion algorithms, based on peak backscattered power and the shape of radio signal waveforms (ESA 2016). However, ground monitors are sparse in space, and the satellites cannot monitor winds continuously in space and time as they are in low earth orbit. Winds in the upper level of the atmosphere can be observed using weather balloons or aircraft measurements, but these observations are also very sparse in space and time.

There is a significant statistical literature on modeling winds from ground monitors (Priestley 1981, Haslett & Raftery 1989, Brillinger 2001, Stein 2005*b*). For some applications, it is sufficient to look at the evolution of wind at a fixed location, and several methods

have been proposed for this scenario (Brown et al. 1984, Tol 1997, Ailliot 2004, Monbet et al. 2007). The wind at different locations can be utilized to model spatio-temporal dependencies (Bennett 1979, Bras & Rodriguez-Iturbe 1985, Kyriakidis & Journel 1999, De Luna & Genton 2005). Also, Boukhanovsky et al. (2003), Malmberg et al. (2005) and Ailliot et al. (2006) proposed autoregressive space-time models to describe the evolution of winds. Stein (2005*b*) proposed a spectral-in-time modeling approach to describe the space-time dependencies of the data. Fuentes et al. (2008) modeled a drift process using Bayesian analysis, where the drift parameter is modeled using splines. Modlin et al. (2012) used circular conditional autoregressive models for wind direction and speed. Sigrist et al. (2012) modeled precipitation with a non-separable spatio-temporal model using an external wind vector.

On the other hand, geostationary weather satellites provide data from the surface and the atmosphere with a very high temporal resolution. The resulting data comprise a series of images which essentially make them a ‘movie’. While the satellites do not directly measure wind, the image sequences are used to infer wind estimates by tracking movements of atmospheric tracers such as clouds or moisture features over time. Wind data obtained from satellite images play a major role in data assimilation. Numerical climate models perform better with accurate wind data, especially over the oceans, resulting in improved weather forecasts and warnings (Tomassini et al. 1999). For example, the European Centre for Medium-Range Weather Forecasts (ECMWF) has been incorporating atmospheric motion winds into their forecast models operationally since the 1980s. This has dramatically improved the model’s ability to forecast the track of tropical cyclones and has also increased the model’s ability to predict wave heights and storm surges (Tomassini et al. 1999).

The Derived Motion Winds (DMW) Algorithm (Daniels et al. 2010) is a standard algorithm for estimating motion winds from satellite images. The DMW Algorithm takes as

input brightness temperature images from the National Oceanic and Atmospheric Administration (NOAA) geostationary meteorological satellites and gives estimated wind fields as outputs. The algorithm tracks a suitable target across the input images and assigns a motion wind to the middle time point (see Section 2 for details). The image at the middle time point must satisfy a set of criteria to qualify as a suitable target scene. As a result, the DMW estimates are often missing. The DMW algorithm also does not produce a measure of uncertainty.

Geostatistical methods are capable of overcoming these shortcomings. This motivates us to model satellite image data using a spatial process drifting in time. At the heart of this statistical model lies the idea of incorporating the motion vector parameters in the process covariance. Stein et al. (2013) uses this idea to fit a space-time model. We borrow the idea of Nested Tracking from Daniels et al. (2010) by considering data buffers and estimate local wind vectors using maximum likelihood estimates over sliding windows over space. Local estimation of covariance parameters using moving windows has been studied in Haas (1990, 1995). One major advantage of our approach over the DMW algorithm is that it allows us to quantify uncertainties in the local estimates of the winds; this in turn facilitates our use of an inverse-variance-weighted spatial smoothing algorithm to borrow strength across space while down-weighting the most uncertain estimates.

## 2 Derived Motion Winds Algorithm

The Derived Motion Winds (DMW) Algorithm estimates atmospheric motion winds from images taken by geostationary satellites. For a cloudy region, the imager records brightness temperature (see Figure 3), which measures the radiance (in Kelvin) of microwave radiation traveling upward from the top of the atmosphere to the satellite. For clear sky portions,

the satellite records images of suitable indicators of atmospheric moisture content, such as specific humidity. Daniels et al. (2010) provides a description of and the physical basis for the estimation of atmospheric winds from the images taken by geostationary satellites.

The DMW algorithm involves creating a *data buffer*, which is a data structure holding 2-dimensional arrays of the response variable for 3 consecutive image times. The middle portion of the buffer is divided into smaller target scenes (or target windows), and each scene is analyzed to locate and select a set of suitable targets in the middle image.

Daniels et al. (2010) gives a description of the Nested Tracking Algorithm which involves nesting smaller target windows (usually of size  $5 \times 5$ ) within a large target scene of size  $15 \times 15$  pixels and getting every possible local motion vectors derived from each possible smaller window within a large target scene. The displacement vector between time points  $t$  and  $t + 1$  is computed by minimizing the Sum of Squared Differences (SSD) criterion as

$$\hat{\mathbf{v}}(\mathbf{x}, t, t + 1) = \underset{\mathbf{u}}{\operatorname{argmin}} \sum_{\mathbf{s} \in D_{\mathbf{x}}} \{Y(\mathbf{s}, t) - Y(\mathbf{s} + \mathbf{u}, t + 1)\}^2,$$

where  $Y(\mathbf{s}, t)$  denotes the brightness temperature within the smaller window at pixel location  $\mathbf{s}$  and time point  $t$ ,  $D_{\mathbf{x}}$  is the indices of pixels in the window centered at  $\mathbf{x}$ , and  $\mathbf{u}$  is a two-dimensional vector denoting the displacement. The sum is considered over two dimensions and the optimization over  $\mathbf{u}$  is done only over integers so that  $\mathbf{s} + \mathbf{u}$  corresponds to an observed pixel. In practice, the search region is substantially larger than the size of the smaller target window, so the above summation is carried out for all target window positions within the search region. The mean displacement vector is computed as

$$\hat{\mathbf{u}}(\mathbf{x}, t) = \frac{1}{2} \{ \hat{\mathbf{v}}(\mathbf{x}, t - 1, t) + \hat{\mathbf{v}}(\mathbf{x}, t, t + 1) \}$$

and is assigned as the DMW estimate at location  $\mathbf{x}$  time point  $t$  in the buffer. Once every possible local motion vectors within the buffer are calculated, a density-based cluster

analysis algorithm, DBSCAN (Ester et al. 1996) is used to identify the largest cluster representing the dominant motion. The final DMW estimate for the buffer is the average of the vectors belonging to the largest cluster.

The size of the target window depends on the spatial and temporal resolution of the imagery and the scale of the intended feature to be tracked. Daniels et al. (2010) suggests that the temporal resolution of the images should at most be 15 minutes in order to account for the short lifespan and rapid disintegration of clouds over land. The DMWA does not offer wind estimates at every  $(\mathbf{x}, t)$  as the data in the middle image has to satisfy a set of criteria to qualify as a suitable target scene. Also, quantifying uncertainties using the SSD criterion is hard because each estimated vector uses a different subset of the data, so likelihood ratio tests are not applicable. Finally, the vector estimates generated for each target scene can at most be half-integers.

### 3 Model-based wind estimation

#### 3.1 Space-time drift models

The proposed approach uses spatio-temporal covariance functions to track the wind. This requires us to consider asymmetric spatio-temporal covariance functions. Space-time asymmetries in covariance functions have been studied in Stein (2005*a*), Huang & Sun (2019) and Park & Fuentes (2006).

The space-time process  $Z(\mathbf{x}, t)$  has asymmetric covariance if

$$\text{Cov}\{Z(\mathbf{x}, t_1), Z(\mathbf{y}, t_2)\} \neq \text{Cov}\{Z(\mathbf{x}, t_2), Z(\mathbf{y}, t_1)\}. \quad (1)$$

In most regions, winds flow in a consistent direction, and so changes in temperature or precipitation rate at one location tend to precede similar changes down wind. For instance,

if  $t_2 > t_1$  and winds flow consistently from  $\mathbf{x}$  to  $\mathbf{y}$ , then we expect

$$\text{Cov}\{Z(\mathbf{x}, t_1), Z(\mathbf{y}, t_2)\} > \text{Cov}\{Z(\mathbf{x}, t_2), Z(\mathbf{y}, t_1)\}.$$

We incorporate space-time asymmetries via a drift parameter. Suppose that  $Z_0$  is a stationary, space-time symmetric process with covariance function

$$C_0(\mathbf{d}, h) = \text{Cov}\{Z_0(\mathbf{x}, t), Z_0(\mathbf{x} + \mathbf{d}, t + h)\},$$

and let

$$Z(\mathbf{x}, t) = Z_0(\mathbf{x} - \mathbf{u}t, t).$$

Then the covariance function of  $Z(\mathbf{x}, t)$  is

$$\begin{aligned} \text{Cov}\{Z(\mathbf{x}, t_1), Z(\mathbf{y}, t_2)\} &= \text{Cov}\{Z_0(\mathbf{x} - \mathbf{u}t_1, t_1), Z_0(\mathbf{y} - \mathbf{u}t_2, t_2)\} \\ &= \sigma^2 C_0\{\mathbf{y} - \mathbf{x} - \mathbf{u}(t_2 - t_1), t_2 - t_1\}, \end{aligned} \tag{2}$$

which is space-time asymmetric and stationary. The parameter  $\mathbf{u}$ , which is a two-dimensional vector representing the zonal and meridional components of the wind, can be interpreted as the drift of the process over time.

### 3.2 Local estimation of the drift parameter

Assume the brightness temperature data  $Y(\mathbf{x}, t)$  are normally distributed and have been standardized to have mean zero and variance one at each location (as described in the Appendix) and denote the standardized data as  $Z(\mathbf{x}, t)$ . The mean and variance carry no information about the drift, and this step simplifies estimation of the covariance parameters. We do not specify the global covariance function for  $Z$ . Instead, we specify its local covariance with drift parameter  $\mathbf{u}(\mathbf{x}, t)$  and estimate the motion winds locally.

We define a target window as a square array of pixels

$$D(\mathbf{x}, t) = \{(\mathbf{x}', t') \text{ such that } \|\mathbf{x} - \mathbf{x}'\|_\infty < \epsilon \text{ \& } |t - t'| \leq 1\}.$$

To estimate  $\mathbf{u}(\mathbf{x}, t)$ , we assume that the process  $Z(\mathbf{x}, t)$  is locally stationary in  $D(\mathbf{x}, t)$  and that winds are smooth enough to be assumed constant in the scene, that is,  $\mathbf{u}(\mathbf{x}', t') \approx \mathbf{u}(\mathbf{x}, t)$  for all  $(\mathbf{x}', t') \in D(\mathbf{x}, t)$ . In other words, we approximate the local covariance function as

$$\text{Cov}\{Z(\mathbf{x}_1, t_1), Z(\mathbf{x}_2, t_2)\} \approx C_0(\mathbf{d} - \mathbf{u}(\mathbf{x}, t)h, h).$$

where  $\mathbf{d} = \mathbf{x}_2 - \mathbf{x}_1$  denotes the spatial lag,  $h = t_2 - t_1$  denotes the temporal lag and  $(\mathbf{x}_1, t_1)$  and  $(\mathbf{x}_2, t_2) \in D(\mathbf{x}, t)$ . In particular, we assume

$$\text{Cov}\{Z(\mathbf{x}_1, t_1), Z(\mathbf{x}_2, t_2)\} = \exp \left( -\sqrt{\frac{\|\mathbf{d} - \mathbf{u}(\mathbf{x}, t)h\|^2}{\alpha_1^2(\mathbf{x}, t)} + \frac{|h|^2}{\alpha_2^2(\mathbf{x}, t)}} \right) \quad (3)$$

Here,  $\alpha_1^2$  and  $\alpha_2^2$  denote respectively the spatial and temporal range parameters. Let  $\boldsymbol{\theta}(\mathbf{x}, t) = (\alpha_1(\mathbf{x}, t), \alpha_2(\mathbf{x}, t), \mathbf{u}(\mathbf{x}, t))$  be the four correlation parameters to be estimated.

We use maximum likelihood estimation within  $D(\mathbf{x}, t)$  to estimate  $\boldsymbol{\theta}(\mathbf{x}, t) \equiv \boldsymbol{\theta}_D$ . That is, if  $\mathbf{Z}_D$  denotes the standardized data vector in the target window and  $\Sigma(\boldsymbol{\theta}_D)$  denote the corresponding space-time covariance matrix with elements defined by (3), then the log-likelihood for  $\boldsymbol{\theta}_D$  given  $\mathbf{Z}_D$  is

$$l(\boldsymbol{\theta}_D | \mathbf{Z}_D) = -\frac{1}{2} \log(|\Sigma(\boldsymbol{\theta}_D)|) - \frac{1}{2} \mathbf{Z}_D^T \{\Sigma(\boldsymbol{\theta}_D)\}^{-1} \mathbf{Z}_D. \quad (4)$$

The estimates obtained are associated with the location  $\mathbf{x}$  and time point  $t$  at which the target window  $D$  was centered, denoted  $\hat{\mathbf{u}}(\mathbf{x}, t)$ . We also estimate the variances associated with the estimated wind vectors by computing the observed inverse Hessian matrix at the maximum likelihood estimate. We imitate the Nested Tracking approach and slide the



target window across space and time, estimating wind vectors locally in space and time using the same optimization routine.

### 3.3 Smoothing the local estimates

After obtaining the local estimates of  $\mathbf{u}(\mathbf{x}, t)$  for all  $(\mathbf{x}, t)$ , we smooth these initial estimates to stabilize them by borrowing strength across space. The two components of the wind vectors are smoothed separately. The kernel smoothing weights are taken to be proportional to the ratio of a spatial Gaussian kernel and the variance of the initial estimate. Full details are given in the Appendix. The bandwidth is chosen based on cross validation.

The size of the target window is an important tuning parameter in the study. While implementing the method on real data sets, the window size should be chosen such that the wind motion is roughly constant in the scene, and the feature being tracked in time is prominent and does not move out of frame. In Section 4, we perform a simulation study analyzing the effect of the model parameters including window size on the performance of our method. We also analyze the efficacy of spatial smoothing of the local estimates. While implementing the methods in the real-data analysis in Section 5, the optimal window size is chosen using cross validation. This works well as wind fields are mostly smooth over a fairly small region and time frame.

## 4 Simulation study

### 4.1 Sensitivity analysis of model parameters

In the first part of our simulation study, we determine the conditions under which the space-time drift model (STDm) performs well for estimating motion winds. For this purpose, we

repeatedly simulate data sets within one particular target window (as opposed to scanning across a spatial domain). We also implement a version of the DMW algorithm and compare its performance with the STDM. To compare the two methods, accuracy for simulated data set  $i$  is measured by Vector Difference (Daniels et al. 2010) between the true ( $\mathbf{u}_0$ ) and estimated ( $\hat{\mathbf{u}}_i$ ) wind vectors

$$VD_i = \|\hat{\mathbf{u}}_i - \mathbf{u}_0\|,$$

and we report the Mean Vector Difference over  $N$  data sets

$$MVD = \frac{1}{N} \sum_{i=1} VD_i$$

and the standard deviation in Table 1.

First we consider data in target windows of size  $7 \times 7 \times 3$  generated independently from the STDM under various parameter settings. The true spatial range parameter  $\alpha_1^2$  is chosen to be either 1, 2, 4 or 8 and the true temporal range parameter  $\alpha_2^2$  is chosen to be either 1, 2, 3 or 4. We also take two different values of the reference wind vector, namely  $\mathbf{u}_0 = (1, 2)^T$  and  $(3, 5)^T$ , which signify respectively slow and fast wind vectors. All four parameters are updated simultaneously during optimization. Table 1 shows the performance of the two methods for the two wind vectors based on  $N = 100$  simulations.

Table 1: Comparing Mean Vector Difference (SD) for Space-time Drift Model (STDM) and Derived Motion Winds algorithm (DMWA) for true wind vectors  $\mathbf{u}_0 = (1, 2)^T$  (left panel) and  $\mathbf{u}_0 = (3, 5)^T$  (right panel) based on data windows of size  $7 \times 7$  (top panel),  $11 \times 11$  (middle panel) and  $15 \times 15$  (bottom panel);  $\alpha_1^2$  and  $\alpha_2^2$  denote the true spatial and temporal range respectively. MVD and SD are measured in pixels.

Window size	MVD of STDM for $\mathbf{u}_0 = (1, 2)^T$					MVD of STDM for $\mathbf{u}_0 = (3, 5)^T$				
	$\alpha_1^2 \backslash \alpha_2^2$	1	2	3	4	$\alpha_1^2 \backslash \alpha_2^2$	1	2	3	4
$7 \times 7$	1	1.196 (0.35)	0.311 (0.22)	0.243 (0.24)	0.201 (0.20)	1	2.310 (1.60)	2.034 (1.66)	1.734 (1.68)	1.787 (1.95)
	2	1.658 (1.13)	0.600 (0.52)	0.353 (0.33)	0.245 (0.12)	2	2.335 (1.56)	2.032 (1.76)	1.392 (1.47)	1.030 (1.21)
	4	2.841 (1.75)	1.599 (1.24)	0.861 (0.61)	0.456 (0.31)	4	3.440 (2.34)	2.393 (1.90)	1.996 (1.70)	1.638 (1.99)
	8	3.253 (2.25)	3.281 (1.87)	2.212 (1.71)	1.432 (1.02)	8	3.611 (2.66)	3.135 (1.92)	2.913 (1.88)	2.483 (2.39)
	MVD of DMWA for $\mathbf{u}_0 = (1, 2)^T$					MVD of DMWA for $\mathbf{u}_0 = (3, 5)^T$				
	$\alpha_1^2 \backslash \alpha_2^2$	1	2	3	4	$\alpha_1^2 \backslash \alpha_2^2$	1	2	3	4
	1	1.983 (1.05)	1.209 (0.85)	1.039 (1.12)	0.854 (1.09)	1	5.953 (0.91)	5.924 (0.96)	5.953 (1.10)	6.012 (0.98)
	2	2.045 (1.02)	1.527 (0.94)	1.283 (1.01)	1.072 (0.98)	2	5.710 (1.09)	5.781 (1.18)	5.899 (1.09)	5.739 (1.08)
$11 \times 11$	4	2.342 (0.94)	2.158 (0.94)	1.620 (0.92)	1.511 (0.91)	4	5.665 (1.09)	5.577 (1.16)	5.540 (1.21)	5.355 (1.13)
	8	2.452 (1.07)	2.175 (0.95)	2.003 (1.10)	1.776 (0.89)	8	5.952 (1.13)	5.678 (1.23)	5.413 (1.12)	5.461 (1.18)
	MVD of STDM for $\mathbf{u}_0 = (1, 2)^T$					MVD of STDM for $\mathbf{u}_0 = (3, 5)^T$				
	$\alpha_1^2 \backslash \alpha_2^2$	1	2	3	4	$\alpha_1^2 \backslash \alpha_2^2$	1	2	3	4
	1	0.415 (0.37)	0.172 (0.09)	0.136 (0.07)	0.118 (0.05)	1	1.124 (1.09)	0.868 (1.50)	0.743 (1.57)	0.530 (1.06)
	2	1.225 (1.21)	0.304 (0.19)	0.162 (0.09)	0.149 (0.08)	2	1.916 (1.69)	0.777 (1.24)	0.299 (0.42)	0.230 (0.41)
	4	3.010 (2.56)	1.008 (0.72)	0.398 (0.25)	0.268 (0.14)	4	2.820 (1.98)	1.489 (1.36)	0.676 (0.70)	0.392 (0.37)
	8	3.441 (3.48)	2.830 (2.06)	1.346 (1.00)	0.831 (0.69)	8	3.401 (2.84)	3.125 (1.96)	2.071 (1.80)	1.129 (1.03)
$15 \times 15$	MVD of DMWA for $\mathbf{u}_0 = (1, 2)^T$					MVD of DMWA for $\mathbf{u}_0 = (3, 5)^T$				
	$\alpha_1^2 \backslash \alpha_2^2$	1	2	3	4	$\alpha_1^2 \backslash \alpha_2^2$	1	2	3	4
	1	1.965 (1.17)	0.771 (0.91)	0.162 (0.50)	0.084 (0.42)	1	5.823 (1.62)	5.836 (1.43)	5.866 (1.59)	6.024 (1.61)
	2	2.230 (1.30)	1.343 (1.08)	0.727 (0.82)	0.409 (0.69)	2	5.638 (1.74)	5.294 (1.75)	5.408 (1.80)	5.362 (1.64)
	4	2.532 (1.32)	1.888 (1.18)	1.856 (1.17)	1.101 (0.86)	4	5.548 (1.42)	4.995 (1.65)	4.934 (1.85)	4.750 (1.70)
	8	2.891 (1.54)	2.538 (1.33)	2.064 (1.09)	1.961 (1.19)	8	5.864 (1.62)	5.320 (1.72)	5.233 (1.75)	4.603 (1.70)

		MVD of STDM for $\mathbf{u}_0 = (1, 2)^T$					MVD of STDM for $\mathbf{u}_0 = (3, 5)^T$				
15 × 15	$\alpha_1^2 \backslash \alpha_2^2$	1	2	3	4		$\alpha_1^2 \backslash \alpha_2^2$	1	2	3	4
	1	0.274 (0.32)	0.125 (0.06)	0.097 (0.05)	0.073 (0.04)		1	0.581 (1.16)	0.403 (1.21)	0.355 (0.88)	0.291 (0.99)
	2	0.803 (0.71)	0.197 (0.11)	0.122 (0.07)	0.103 (0.05)		2	1.073 (1.14)	0.244 (0.13)	0.142 (0.07)	0.107 (0.06)
	4	2.443 (1.64)	0.536 (0.40)	0.251 (0.14)	0.183 (0.08)		4	2.781 (2.21)	0.690 (0.65)	0.307 (0.18)	0.211 (0.11)
	8	3.268 (3.60)	2.030 (2.05)	0.875 (0.59)	0.496 (0.35)		8	3.175 (3.46)	2.721 (2.55)	1.123 (0.97)	0.665 (0.53)
	MVD of DMWA for $\mathbf{u}_0 = (1, 2)^T$						MVD of DMWA for $\mathbf{u}_0 = (3, 5)^T$				
	$\alpha_1^2 \backslash \alpha_2^2$	1	2	3	4		$\alpha_1^2 \backslash \alpha_2^2$	1	2	3	4
	1	2.998 (1.55)	1.501 (1.56)	0.699 (1.33)	0.318 (0.84)		1	5.100 (2.54)	2.830 (2.46)	0.688 (1.54)	0.098 (0.62)
	2	2.776 (1.42)	2.028 (1.40)	1.365 (1.57)	0.815 (1.18)		2	5.306 (2.43)	3.417 (2.51)	1.819 (2.16)	1.028 (1.77)
	4	3.213 (1.69)	2.661 (1.67)	2.236 (1.67)	1.644 (1.47)		4	5.724 (2.47)	3.951 (2.42)	3.378 (2.37)	2.670 (2.32)
	8	3.579 (1.70)	2.921 (1.39)	2.700 (1.53)	2.518 (1.34)		8	6.109 (2.26)	5.15 (2.44)	4.393 (2.33)	4.061 (2.56)

STDM does a better job in estimating moderately small and large wind vectors for the  $7 \times 7$  window size compared to DMWA. Mean vector distance is the smallest when the true spatial range is small and the true temporal range is large. This is intuitive because a small spatial range makes it easier to identify a feature in the target scene, and a large temporal range means that the features dissipate slowly over time. STDM also performs better for the smaller wind vector because when the wind vector is large compared to the window size, the feature tracked in time could potentially move out of the frame, resulting in incorrect wind estimates. In particular, windows of size  $7 \times 7$  are not adequate to contain the features being tracked in frame for a wind vector of  $(3, 5)^T$  which is reflected in the high MVD and SD values for STDM (see Table 1, top panel).

The performance of the DMW algorithm also improves as the temporal range increases. However, these simulation results bring forth a major flaw in the DMW algorithm. The estimated motion winds from the DMW algorithm are at most half integers and they are limited to the size of the larger search window. That is, while estimating the motion vectors, the smaller central target scene ( $3 \times 3$ ) can only move up to 4 pixels in all directions while it is being tracked back and forward in time. As a result, it performs poorly for the larger

wind motion vector, which had a v-component of 5 pixel units. This can once again be attributed to the window size relative to the magnitude of the wind vector.

To examine the effect of window size, we now perform the simulations again with window sizes of  $11 \times 11$  and  $15 \times 15$  respectively, under the same covariance parameter settings as described earlier. The panels of Table 1 portray a clear picture of the effect of window size on the estimation of winds using STDm. The estimation of both wind vectors improve as we increase window size from  $7 \times 7$  to  $11 \times 11$  (see Table 1, middle panel) and then to  $15 \times 15$  (see Table 1, bottom panel).

In this simulation, a larger target window always produces more accurate estimates of the wind components. However, this might not be the case in practice. In this part of the simulation study, the true winds have been chosen in a single window. When we consider a spatial domain, choosing an arbitrarily large target window might lead to inaccurate estimates of the wind vectors. In the next part of the simulation study, we look at motion winds over a spatial domain.

## 4.2 Efficacy of spatial smoothing

We now conduct another simulation study which examines the efficacy of spatial smoothing of wind estimates. For this purpose, we generate data sets on a unit square of size  $60 \times 60$  and for three consecutive time points, as opposed to focusing on one particular target window. We consider two types of true winds while generating the data. In the first case, we consider constant winds over the space-time domain. In particular, we consider

$$\begin{pmatrix} u_1 \\ u_2 \end{pmatrix} = \begin{pmatrix} 0.058 \\ 0.058 \end{pmatrix}.$$

This is an extension of the simulation setting in Section 4.1 and is equivalent to considering the translation warping function (Majumder et al. 2019). Next, we consider rotational winds, which are obtained by rotating each location counter-clockwise by  $6^\circ$  at each time point. These winds are non-uniform over space and emulate big tropical storms which rotate counter-clockwise in the Northern Hemisphere and clockwise in the Southern Hemisphere due to the Coriolis effect. Thus, both cases reflect realistic scenarios and compensate for the lack of availability of data sets with ground truth for wind measurements.

For each of the two scenarios, the shifted locations are obtained at three consecutive time points. A fast Gaussian approximation algorithm (Guinness 2018) is then implemented using the ‘GpGp’ package (Guinness & Katzfuss 2018) in R to generate the data sets for the three consecutive time points. We use the exponential space-time covariance function, given in equation (3) with true spatial range  $\alpha_1^2 = 0.075$  (4 pixels) and true temporal range  $\alpha_2^2 = 15$ . We estimate the parameters locally using maximum likelihood estimation. The wind estimates are spatially smoothed using a weighted kernel with suitable bandwidth. We also estimate the winds using DMW algorithm, and the DMWA estimates are also smoothed for fair comparison.

As discussed earlier, the size of the target window plays a crucial role while estimating motion winds. A target window of size  $15 \times 15$  is adequate to estimate the constant wind field by tracking features across three consecutive time points. However, while estimating the rotational wind field using  $15 \times 15$  windows, some of the target features move out of scene because of the non-uniformity in winds across space. In that scenario, both methods provide poor estimates of the wind field. As a result, we use target windows of size  $25 \times 25$  while estimating the rotational wind field. Table 2 compares the average performance of the algorithms and their smoothed versions over  $N = 100$  simulated data sets. Figures 1 and 2 show the respective true wind fields (in red) along with the raw and smoothed

Table 2: Comparing Mean Vector Difference (SD) for raw and smoothed wind estimates from the Space-Time Drift Model (STDM) and the Derived Motion Winds Algorithm (DMWA) averaged over  $N = 100$  data sets simulated using constant and rotational wind fields. MVD and SD are measured in pixels.

Method	Constant ( $15 \times 15$ )	Rotation ( $25 \times 25$ )
STDM	0.061 (0.034)	0.257 (0.108)
DMWA	0.805 (1.08)	0.349 (0.163)
Smoothed STDM	<b>0.056 (0.032)</b>	<b>0.256 (0.108)</b>
Smoothed DMWA	0.546 (0.437)	0.266 (0.112)

estimates obtained using both algorithms (in blue) for a single representative data set. The wind vectors are plotted for a subset of the  $60^2$  locations in the spatial domain for clear visualization of the true and estimated fields.

From the results, it can be seen that the STDM performs better than the DMWA in both scenarios. Also, smoothing the estimates gives us a much better representation of the wind fields compared to the raw estimates. While estimating non-uniform wind fields, selecting the window size requires balancing a trade-off between a window size that is large enough to capture targets moving through the scene yet small enough to satisfy the assumption that within the window the process is stationary with a constant drift. This motivates us to choose the window size using cross validation in the real-data analysis.

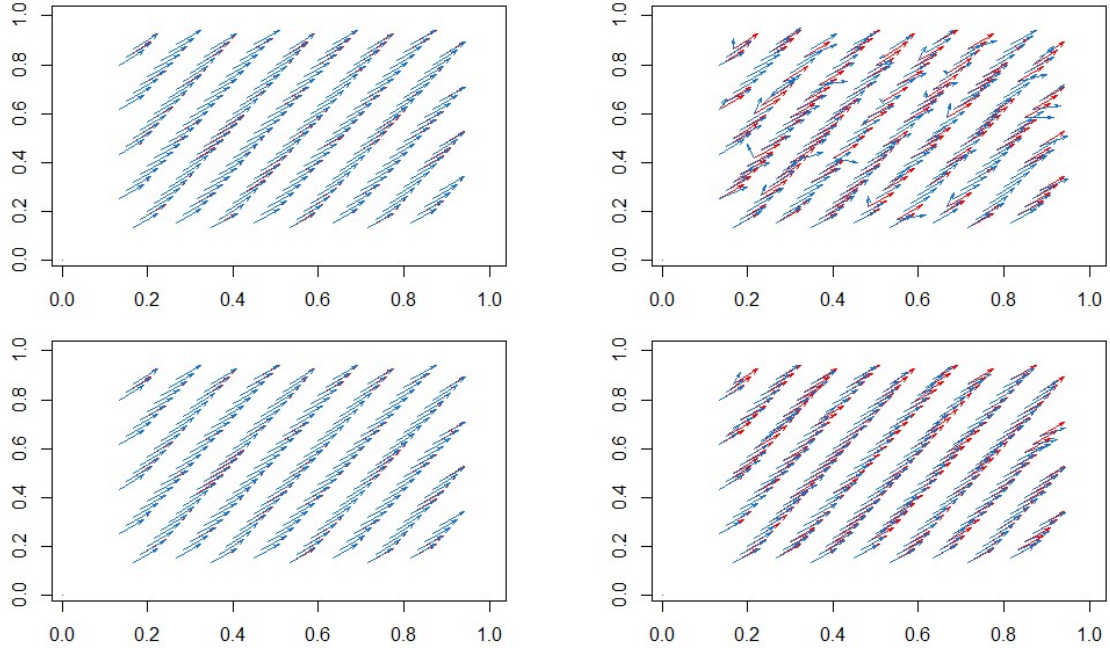


Figure 1: True (red) and estimated (blue) wind fields using Space-Time Drift Model (left column) and Derived Motion Winds Algorithm (right column) for one representative data set, simulated using constant wind field. The top row shows the raw estimates from the two methods, the bottom row shows the smoothed estimates. The wind vectors are plotted for a subset of spatial locations for clear visualization.



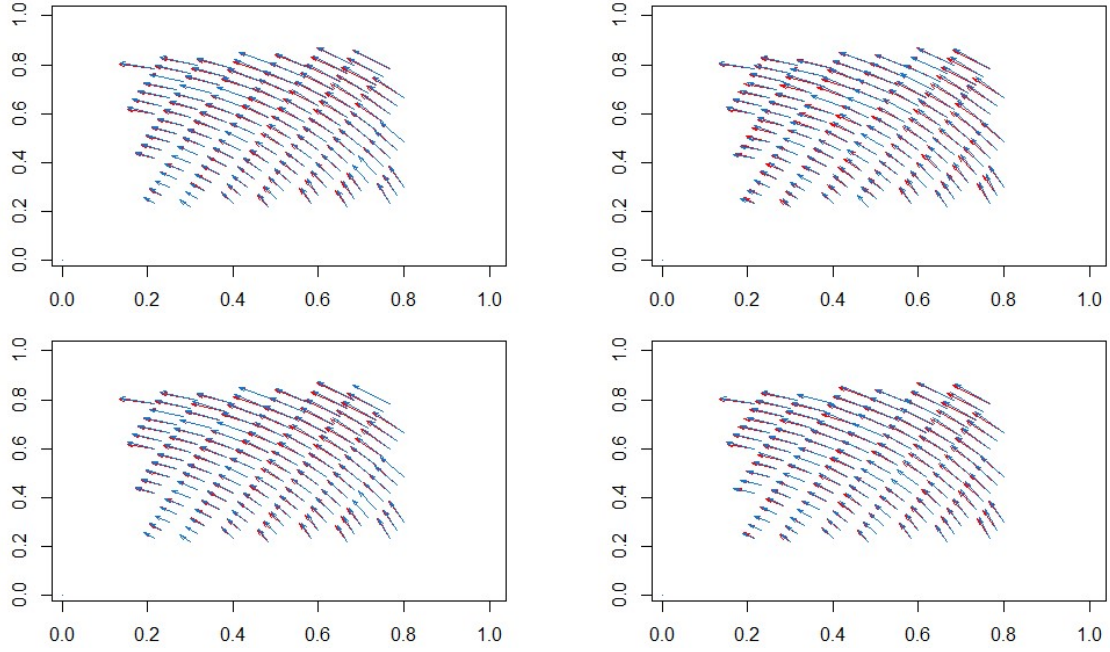


Figure 2: True (red) and estimated (blue) wind fields using Space-Time Drift Model (left column) and Derived Motion Winds Algorithm (right column) for one representative data set, simulated using rotational wind field. The top row shows the raw estimates from the two methods, the bottom row shows the smoothed estimates. The wind vectors are plotted for a subset spatial locations for clear visualization.

## 5 Application to GOES-15 data

### 5.1 GOES-15 data description

The Geostationary Operational Environmental Satellite (GOES), operated by NOAA provides continual measurements of the atmosphere and surface variables, which help facilitate meteorological research including weather forecasting and severe storm tracking. Since the launch of GOES-8 in 1994, the GOES instruments have monitored atmospheric phenomena and provided a continuous stream of environmental data. The data set used in this project is from the GOES-15 satellite. Launched in March 2010, GOES-15 is positioned at the GOES-West location of  $135^{\circ}\text{W}$  longitudes over the Pacific Ocean. The data set, as described in Knapp & Wilkins (2018), is a gridded satellite Contiguous US domain data which are geostationary data remapped to equal angle projection with an  $0.04^{\circ}$  ( $\sim 4$  km) latitudinal resolution and 15 minutes temporal resolution. The data set includes infrared channel data in terms of pixel-wise brightness temperature for the reflective bands (channels 1 - 6 with approximate central wavelengths 0.47, 0.64, 0.865, 1.378, 1.61, 2.25 microns respectively). The reflective bands support among other ground and atmospheric indicators, the characterization of clouds. Gridded GOES-15 data can be obtained from NOAA One-Stop at <https://data.noaa.gov/onestop/#!/collections>.

We analyze Channel 4 brightness temperature data (recorded in Kelvin scale) for 10 consecutive days starting January 1, 2015 at a temporal resolution of 15 minutes (960 total images), covering a region in Colorado ( $36.82^{\circ}$  N to  $41.18^{\circ}$  N latitudes and  $109.78^{\circ}$  W to  $101.02^{\circ}$  W longitudes). For our analysis, we focus on the region of Northeast Colorado, comprising 6,160 pixels, where we can see clear cloud movements from south-west to north-east. Figure 3 shows the data at three consecutive time points on the third day. Lower values of brightness temperature indicates cloud cover, whereas high brightness temperature

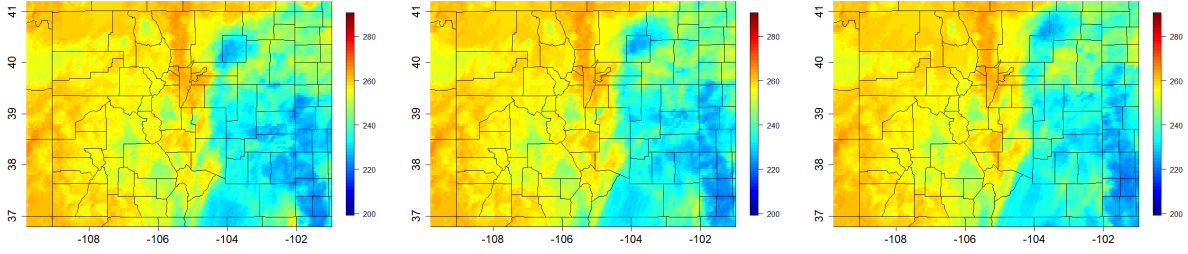


Figure 3: Brightness temperature (Kelvin) maps over Colorado on January 3, 2015 at 00:52 am, 01:07 am and 01:22 am respectively.

values suggest clear skies over the region.

## 5.2 Estimation using GOES-15 data

The first step involves standardizing the brightness temperature data using the pixel-wise sample mean and standard deviation over time. This factors out the effect of low cloud cover over the region which can affect the local estimation of wind vectors. To smooth out the standard deviation map, we use a Gaussian kernel with smoothing parameter  $\lambda = 2$  pixels (i.e., 8 km).

We use cross validation to determine the appropriate size of target windows. With no direct measurement of the wind, we compare window sizes indirectly based on predictions of brightness temperature at the fourth time point using the wind estimate based on the first three time points and use this optimal window size to estimate winds for the subsequent time points. Table 3 gives us the Mean Squared Prediction Error (MSPE) (discussed in Section 5.3) for a few window sizes and the corresponding computation time to estimate the wind vectors at all 6,160 pixels using 4 consecutive time steps. Based on these results, we use window size of  $25 \times 25$  pixels (i.e.,  $100 \text{ km} \times 100 \text{ km}$  regions) and estimate the

Table 3: Mean Squared Prediction Error for cross validation based on the first three time points and the corresponding computation time (in hours)

window size	MSPE	Computation time (in hours)
$11 \times 11$	0.409	1.083
$15 \times 15$	0.276	3.371
$21 \times 21$	0.225	12.76
$25 \times 25$	0.208	24.85
$35 \times 35$	0.214	81.00

wind vectors locally at each spatial location and at each time using maximum likelihood estimates using the data in the window. We also estimate the variances associated with the estimates by computing the inverse Hessian matrix at the MLE. Figure 4 shows the uncertainty associated with the estimated wind components as given by the estimated standard deviations in the log scale, for three consecutive time points.

The estimated standard deviations in Figure 4 are high for some locations, which makes the wind estimates rough. To account for this, we smooth each component of the estimated wind field using weighted Gaussian kernels, the weights being scaled to the inverse variances of the estimates (details are given in the Appendix). The smoothing parameter has been chosen based on cross validation. Figure 5 shows the raw and smoothed wind estimates obtained from the proposed STDm. From Figures 4 and 5, it can be seen that the rough wind estimates correspond to regions where the estimated standard deviation is high. Figure 5 also shows the smoothed estimates. For fair comparison, the DMW estimates are also smoothed using a simple Gaussian kernel smoother with its optimal smoothing parameter

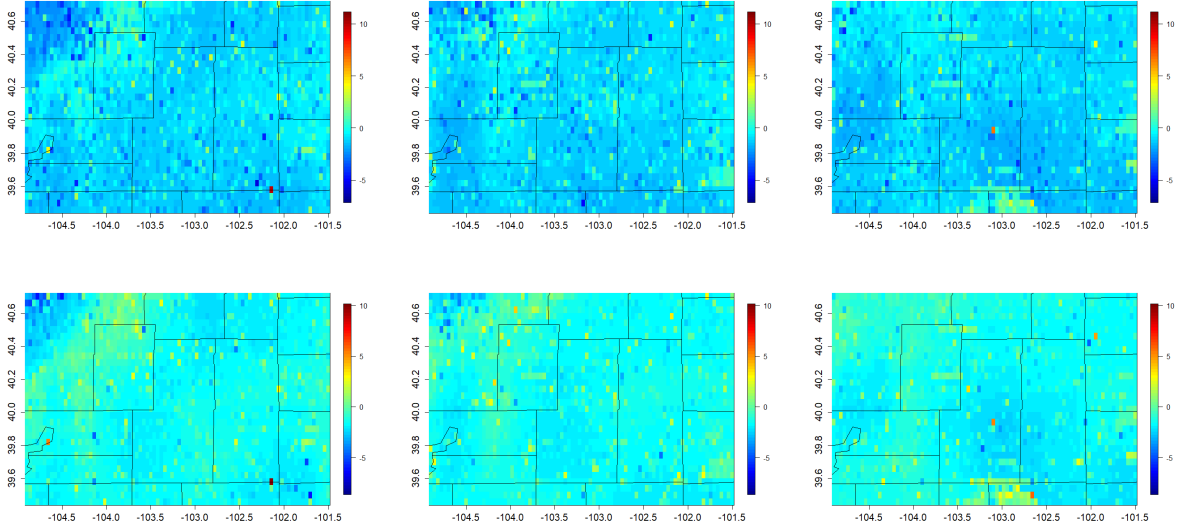


Figure 4: Estimated standard deviations (in log scale) obtained using the Space-Time Drift Model (STDm), corresponding to estimated east-west (top row) and north-south (bottom row) components at three consecutive time points. The columns (from left to right) represent 3 consecutive time points,  $t = 2, 3$  and  $4$  respectively.

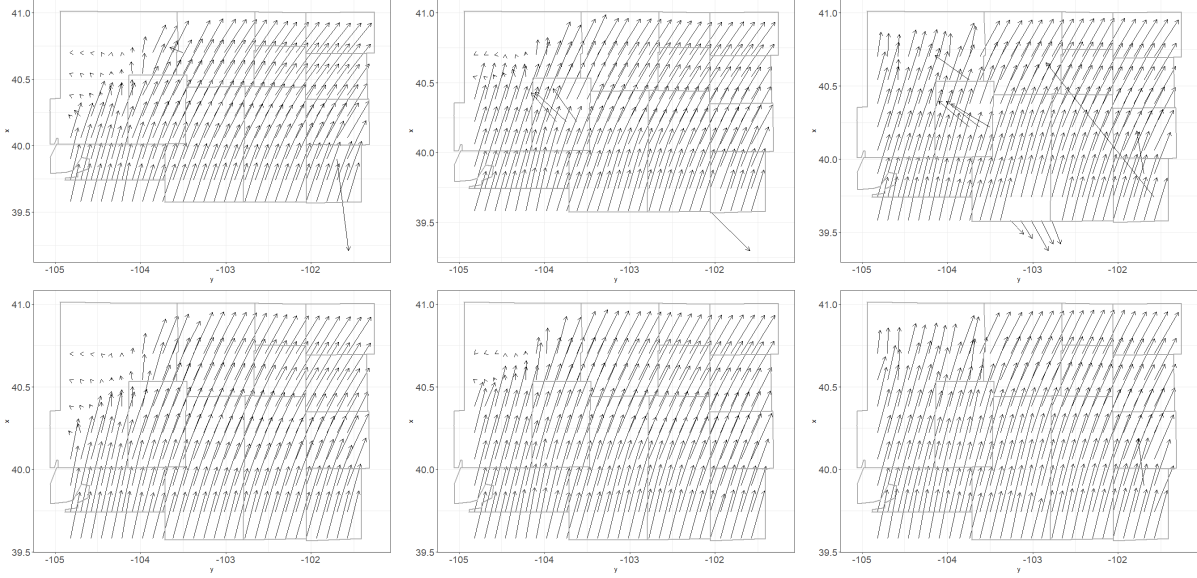


Figure 5: Raw (top row) and smoothed (bottom row) wind field estimates at three consecutive time points obtained using the Space-Time Drift Model (STDM). The columns (from left to right) represent 3 consecutive time points,  $t = 2, 3$  and  $4$  respectively. The background is the county boundaries in northeast Colorado.

chosen using cross validation. The raw and smoothed estimates of the wind fields obtained from DMWA are shown in Figure 6.

### 5.3 Comparison based on Mean Squared Prediction Error

For this dataset, reference wind fields are not available. Hence, we compare the two methods based on Mean Squared Prediction Error (MSPE) while predicting standardized brightness temperature fields. To predict  $Z$  at a spatial location  $\mathbf{x}$  at time  $t$ , we consider  $\mathbf{Z}_D(\cdot, t-1)$ , the standardized data in  $D(\mathbf{x}, t-1)$  and estimated winds at time  $t-2$ . This is because the estimated winds at time  $t-1$  uses data from time  $t$ . The predicted standardized temperature

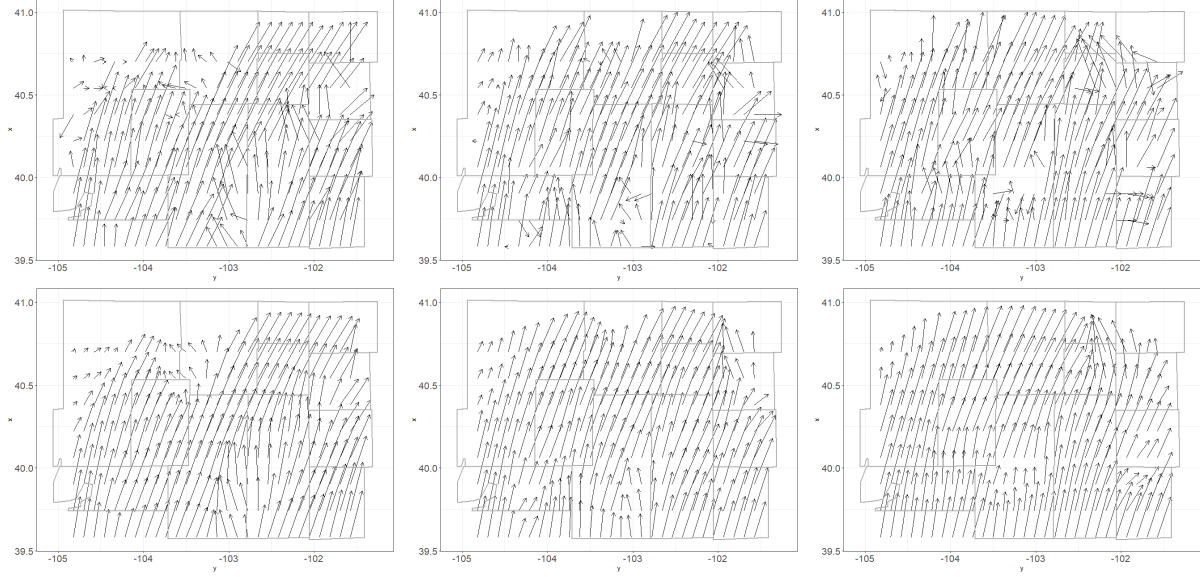


Figure 6: Raw (top row) and smoothed (bottom row) wind field estimates at three consecutive time points, obtained from the Derived Motion Winds Algorithm (DMWA). The columns (from left to right) represent 3 consecutive time points,  $t = 2, 3$  and  $4$  respectively. The background is the county boundaries in northeast Colorado.

Table 4: Comparing Mean Squared Prediction Error based on prediction using the raw and smoothed wind estimates from the Space-Time Drift Model (STDM) and the Derived Motion Winds Algorithm (DMWA) at different time points.  $\lambda$  in each case denotes the optimal smoothing parameter chosen using cross validation. All the methods have been compared against the baseline prediction.

Method	$t = 4$	$t = 5$	$t = 6$	$t = 7$
STDM	<b>0.278</b>	<b>0.195</b>	<b>0.205</b>	<b>0.224</b>
DMWA	0.400	0.293	0.298	0.265
Smoothed STDM ( $\lambda = 2$ km)	<b>0.278</b>	<b>0.195</b>	<b>0.180</b>	<b>0.194</b>
Smoothed DMWA ( $\lambda = 8$ km)	0.364	0.251	0.258	0.214
Baseline	1.275	1.180	0.928	0.812

is calculated as the mean of the Gaussian conditional distribution of  $Z(\mathbf{s}, t)$  given  $\mathbf{Z}_D(\cdot, t - 1)$  under the stationary space-time drift model with estimated drift parameter  $\hat{\mathbf{u}}(\mathbf{s}, t - 2)$ . We also consider a naive approach of predicting the brightness temperature fields, where the data at time  $t - 1$  is considered to be the predicted standardized brightness temperature fields at time  $t$ . We call it the baseline prediction and the performances of the two methods are assessed relative to the baseline MSPE. Table 4 compares the raw and smoothed estimates of the wind components in terms of MSPE.

From Table 4, we can conclude that the proposed model outperforms the DMW algorithm. We also see that smoothing the estimates does provide a better picture of the wind fields over Northeast Colorado. Figure 7 provides maps of predicted standardized brightness temperature using the estimated winds from STDM along with the lower and



upper prediction maps for the brightness temperature fields, calculated using prediction variances. Figure 7 also shows the observed temperature fields for the three consecutive time points. Figure 7 shows that our model captures the main features in the temperature fields over Northeast Colorado. Our model also captures the wind movement over the region since we can see similar movements of features across the region as compared to the ones tracked along in the original images.

## 6 Discussions and Conclusions

Wind is one of the most important atmospheric variables; it has large impact on local weather and hence, studying winds is essential. Wind data can be derived from high-resolution spatiotemporal data collected by geostationary satellites. These data are sequence of images over time and are used to derive atmospheric wind speed and direction. One algorithm that provides wind estimates is known as the Derived Motion Winds Algorithm. It takes as its input a sequence of images taken by the GOES-R series of the NOAA meteorological satellites and produces wind speed and direction. However, this algorithm does not quantify uncertainties. In this paper, we propose a spatiotemporal model to analyze satellite image data with the primary objective of estimating atmospheric wind speed and direction.

We have proposed local estimation of drift parameters. Developing a globally valid nonstationary space time drift model is an interesting problem that we have not pursued here. Following the basic idea of Nested Tracking, we propose a method to estimate the covariance parameters using maximum likelihood estimation. We smooth the raw estimated wind fields using a weighted Gaussian kernel, the weights being scaled by the inverse of the estimated variances of the estimates. Section 4 details an extensive simulation study that

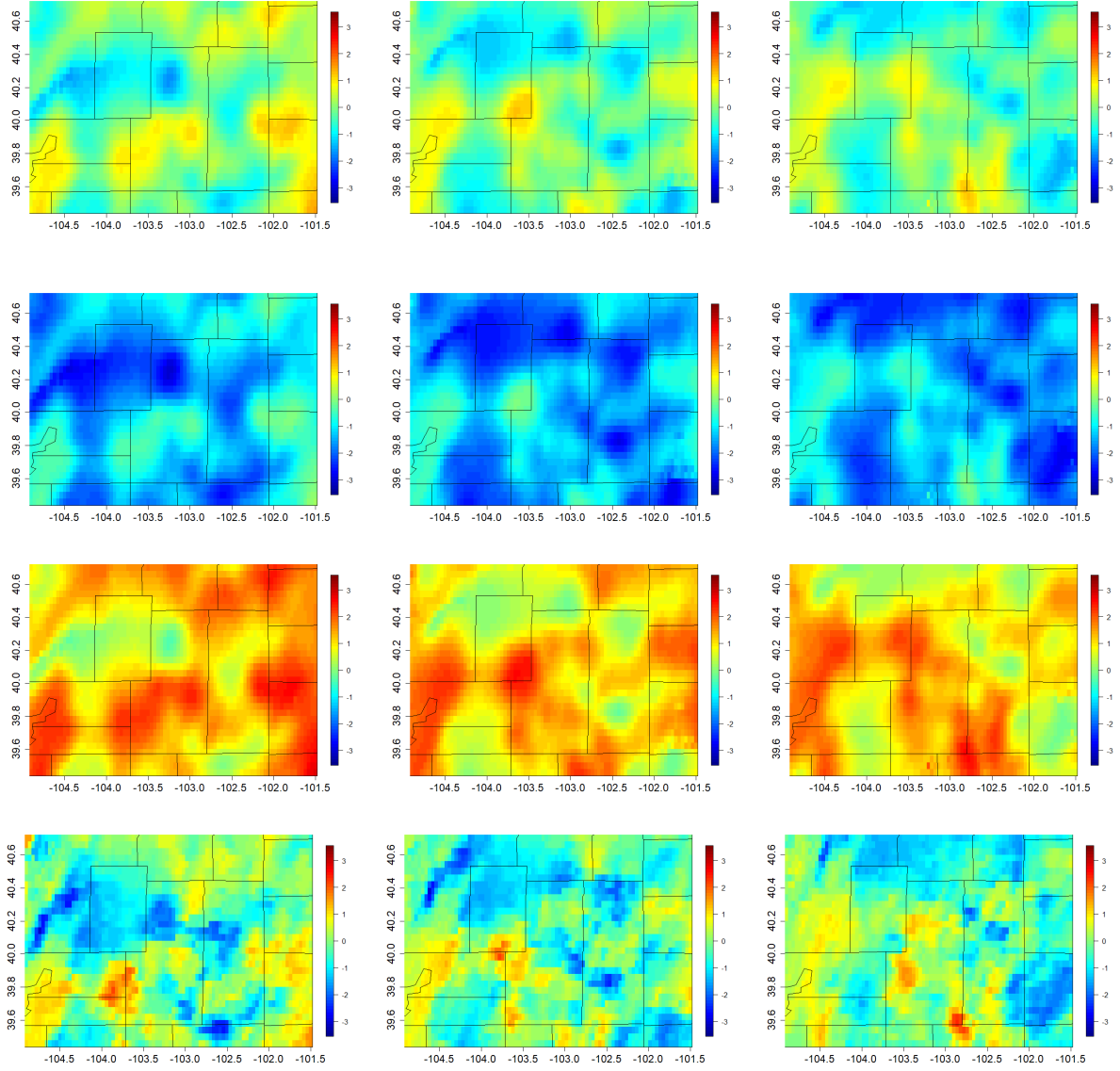


Figure 7: The top row shows predicted (standardized) brightness temperature fields for three consecutive time points, obtained using smoothed wind estimates from the Space-Time Drift Model (STDM). The second and third rows show respectively, the corresponding lower and upper prediction regions. The bottom row shows the observed standardized temperature fields at those time points.

outlines conditions under which our model performs well. Based on our simulation study, we conclude that we have accurate wind estimates when the true spatial correlation range is small and the true temporal correlation range is high. The simulations also show that spatial smoothing provides better estimates of the wind fields. The simulations highlight a major drawback of the DMWA. Due to the design of the DMW algorithm, the local DMWA estimates can only be half-integers and can only take values equal to the number of pixels the smaller target scene can move around in the larger search window. This brings us to perhaps the most important tuning parameter in the analysis, the target window size. We show that the window size is very crucial for both methods with large bias resulting from a large window and variance resulting from a small window.

We apply our method on brightness temperature data over Northeast Colorado, obtained from the GOES-15 satellite. While estimating winds, the window size has been chosen using cross validation. We provide estimated standard deviation maps, showing that our method is capable of quantifying uncertainties associated with the estimation. We also provide smoothed maps of estimated wind fields over Northeast Colorado. We predict brightness temperature fields using our model and compare the raw and smoothed estimates of wind fields based on Mean Squared Prediction Error (MSPE). We also compare the performance of our proposed method and the DMWA. We have shown that our method outperforms the DMWA with respect to MSPE. We argue that smoothing the estimated wind fields give more reliable wind estimates. We also see that we capture the main features in the brightness temperature maps through our prediction, including the drift across the region.

One of the major challenges of our method is to apply it to data in real time. The main computational bottleneck is the time required for optimization over the covariance parameters. Because we use a local likelihood approach, the method is embarrassingly

parallelizable across pixels and time points, and thus should scale well when used in production. The optimization can also be made faster using approximation. For example, the optimization algorithm could be initialized using the results of spatial or temporal neighbors, and the parameters could be updated using a one-step Fisher’s scoring approximation. We would also like to explore more flexible methods for capturing the complicated wind motions, possibly a method where the window size is allowed to vary with location and time. This can ensure that our feature is always inside the frame of reference, resulting in more accurate estimates of the wind fields.

## APPENDIX

*A. Standardization of data:* We standardize the brightness temperature data  $Y(\mathbf{x}, t)$  as

$$Z(\mathbf{x}, t) = \frac{Y(\mathbf{x}, t) - \hat{\mu}(\mathbf{x})}{\hat{\sigma}(\mathbf{x})}$$

where  $\hat{\mu}(\mathbf{x})$  denotes the pixel-wise sample mean over time of  $Y(\mathbf{x}, t)$  at location  $\mathbf{x}$ , and  $\hat{\sigma}(\mathbf{x})$  denotes the corresponding smoothed standard deviation. The standard deviation is smoothed using the Gaussian kernel

$$\phi(\mathbf{x}|\mathbf{v}_l, \lambda) = \frac{1}{2\pi\lambda^2} \exp\left(-\frac{\|\mathbf{x} - \mathbf{v}_l\|^2}{2\lambda^2}\right),$$

where  $\lambda > 0$  is the kernel bandwidth and  $\mathbf{v}_1, \dots, \mathbf{v}_L \in \mathbb{R}^2$  denote the spatial locations over the entire region considered. The smoothing weights are defined as

$$w_l(\mathbf{x}) = \frac{\phi(\mathbf{x}|\mathbf{v}_l, \lambda)}{\sum_{j=1}^L \phi(\mathbf{x}|\mathbf{v}_j, \lambda)}.$$

That is, for standardizing the data we use

$$\hat{\sigma}(\mathbf{x}) = \sum_{l=1}^L \tilde{\sigma}(\mathbf{v}_l) w_l(\mathbf{x}),$$

where  $\tilde{\sigma}(\mathbf{v}_l)$  is the sample standard deviation at location  $\mathbf{v}_l$ .

*B. Smoothing the estimates:* Let  $\hat{\mathbf{u}}(\mathbf{x}, t) = (\hat{u}(\mathbf{x}, t), \hat{v}(\mathbf{x}, t))$  denote the estimated wind vector in  $D(\mathbf{x}, t)$  using the proposed method. Also let the corresponding estimated variances be denoted by  $\hat{d}_u(\mathbf{x}, t)$  and  $\hat{d}_v(\mathbf{x}, t)$  where the suffixes ‘u’ and ‘v’ refer to the u- and v- component of the estimated wind vector. We smooth each component of the estimates using a weighted Gaussian smoothing filter, the weights being equal to the inverses of the corresponding variance estimates. Let  $\hat{\mathbf{u}}^{(s)}(\mathbf{x}, t) = (\hat{u}^{(s)}(\mathbf{x}, t), \hat{v}^{(s)}(\mathbf{x}, t))$  denote the smoothed wind estimates where,

$$\hat{u}^{(s)}(\mathbf{x}, t) = \sum_{l=1}^L \hat{u}(\mathbf{v}_l, t) w_l^u(\mathbf{x}, t), \quad w_l^u(\mathbf{x}, t) = \frac{\left\{ \phi(\mathbf{x}|\mathbf{v}_l, \lambda) / \hat{d}_u(\mathbf{v}_l, t) \right\}}{\sum_{j=1}^L \left\{ \phi(\mathbf{x}|\mathbf{v}_j, \lambda) / \hat{d}_u(\mathbf{v}_j, t) \right\}}$$

$$\hat{v}^{(s)}(\mathbf{x}, t) = \sum_{l=1}^L \hat{v}(\mathbf{v}_l, t) w_l^v(\mathbf{x}, t), \quad w_l^v(\mathbf{x}, t) = \frac{\left\{ \phi(\mathbf{x}|\mathbf{v}_l, \lambda) / \hat{d}_v(\mathbf{v}_l, t) \right\}}{\sum_{j=1}^L \left\{ \phi(\mathbf{x}|\mathbf{v}_j, \lambda) / \hat{d}_v(\mathbf{v}_j, t) \right\}}$$

## References

- Ahmad, N., Suzuki, T. & Banno, M. (2015), ‘Analyses of shoreline retreat by peak storms using Hasaki Coast Japan data’, *Procedia Engineering* **116**, 575–582.
- Ailliot, P. (2004), Modeles autorégressifs a changement de régimes Markovien-Application a la simulation du vent, PhD thesis, PhD Thesis. Université de Rennes 1.
- Ailliot, P., Monbet, V. & Prevosto, M. (2006), ‘An autoregressive model with time-varying coefficients for wind fields’, *Environmetrics* **17**(2), 107–117.
- Bennett, R. J. (1979), ‘Spatial time series’, *Pion, London* **674**.

- Berkowitz, B. & Steckelberg, A. (2017), ‘How Santa Ana winds spread wildfires’, <https://www.washingtonpost.com/graphics/2017/national/santa-ana-fires/>.
- Boukhanovsky, A. V., Krogstad, H. E., Lopatoukhin, L. J. & Rozhkov, V. A. (2003), Stochastic simulation of inhomogeneous metocean fields. part i: Annual variability, *in* ‘International Conference on Computational Science’, Springer, pp. 213–222.
- Bras, R. L. & Rodriguez-Iturbe, I. (1985), *Random functions and hydrology*, Courier Corporation.
- Brillinger, D. R. (2001), *Time series: Data analysis and theory*, Vol. 36, Siam.
- Brown, B. G., Katz, R. W. & Murphy, A. H. (1984), ‘Time series models to simulate and forecast wind speed and wind power’, *Journal of Climate and Applied Meteorology* **23**(8), 1184–1195.
- Castino, F., Festa, R. & Ratto, C. (1998), ‘Stochastic modelling of wind velocities time series’, *Journal of Wind Engineering and Industrial Aerodynamics* **74**, 141–151.
- Daniels, J., Velden, C., Bresky, W., Wanzong, S. & Berger, H. (2010), *GOES-R Advanced Baseline Imager (ABI) Algorithm Theoretical Basis Document for: Derived Motion Winds*, University of Wisconsin–Madison.
- De Luna, X. & Genton, M. G. (2005), ‘Predictive spatio-temporal models for spatially sparse enviromental data’, *Statistica Sinica* **15**, 547–568.
- ESA, E. S. A. (2016), ‘Wind speed’, <https://sentinel.esa.int/web/sentinel/user-guides/sentinel-3-altimetry/overview/geophysical-measurements/wind-speed>.

- Ester, M., Kriegel, H.-P., Sander, J., Xu, X. et al. (1996), A density-based algorithm for discovering clusters in large spatial databases with noise., *in* ‘Kdd’, Vol. 96, pp. 226–231.
- Fuentes, M., Reich, B. J., Lee, G. et al. (2008), ‘Spatial–temporal mesoscale modeling of rainfall intensity using gage and radar data’, *The Annals of Applied Statistics* **2**(4), 1148–1169.
- Guinness, J. (2018), ‘Permutation and grouping methods for sharpening gaussian process approximations’, *Technometrics* .
- Guinness, J. & Katzfuss, M. (2018), ‘Gpgp: Fast gaussian process computation using vecchia’s approximation’, *R package version 0.1. 0* .
- Haas, T. C. (1990), ‘Lognormal and moving window methods of estimating acid deposition’, *Journal of the American Statistical Association* **85**(412), 950–963.
- Haas, T. C. (1995), ‘Local prediction of a spatio-temporal process with an application to wet sulfate deposition’, *Journal of the American Statistical Association* **90**(432), 1189–1199.
- Haslett, J. & Raftery, A. E. (1989), ‘Space-time modelling with long-memory dependence: Assessing Ireland’s wind power resource’, *Applied Statistics* pp. 1–50.
- Huang, H. & Sun, Y. (2019), ‘Visualization and assessment of spatio-temporal covariance properties’, *Spatial Statistics* **34**, 100272.
- Kim, T.-H., Yang, C.-S., Oh, J.-H. & Ouchi, K. (2014), ‘Analysis of the contribution of wind drift factor to oil slick movement under strong tidal condition: Hebei spirit oil spill case’, *PLOS ONE* **9**(1), e87393.

- Knapp, K. R. & Wilkins, S. L. (2018), ‘Gridded satellite (gridsat) GOES and CONUS data’, *Earth System Science Data* **10**(3), 1417–1425.
- Kyriakidis, P. C. & Journel, A. G. (1999), ‘Geostatistical space–time models: A review’, *Mathematical geology* **31**(6), 651–684.
- Majumder, S., Guan, Y., Reich, B. J., O’Neill, S. & Rappold, A. G. (2019), ‘Statistical downscaling with spatial misalignment: Application to wildland fire pm  $_{2.5}$  concentration forecasting’, *arXiv preprint arXiv:1909.12429* .
- Malmberg, A., Holst, U. & Holst, J. (2005), ‘Forecasting near-surface ocean winds with Kalman filter techniques’, *Ocean Engineering* **32**(3-4), 273–291.
- Modlin, D., Fuentes, M. & Reich, B. J. (2012), ‘Circular conditional autoregressive modeling of vector fields’, *Environmetrics* **23**(1), 46–53.
- Monbet, V., Ailliot, P. & Prevosto, M. (2007), ‘Survey of stochastic models for wind and sea state time series’, *Probabilistic engineering mechanics* **22**(2), 113–126.
- Park, M. S. & Fuentes, M. (2006), New classes of asymmetric spatial-temporal covariance models, Technical report, North Carolina State University. Dept. of Statistics.
- Priestley, M. B. (1981), *Spectral analysis and time series*, Academic Press London; New York.
- Sigrist, F., Künsch, H. R., Stahel, W. A. et al. (2012), ‘A dynamic nonstationary spatio-temporal model for short term prediction of precipitation’, *The Annals of Applied Statistics* **6**(4), 1452–1477.



- Stein, M. L. (2005*a*), ‘Space–time covariance functions’, *Journal of the American Statistical Association* **100**(469), 310–321.
- Stein, M. L. (2005*b*), ‘Statistical methods for regular monitoring data’, *Journal of the Royal Statistical Society: Series B (Statistical Methodology)* **67**(5), 667–687.
- Stein, M. L., Chen, J., Anitescu, M. et al. (2013), ‘Stochastic approximation of score functions for Gaussian processes’, *The Annals of Applied Statistics* **7**(2), 1162–1191.
- Tol, R. S. (1997), ‘Autoregressive conditional heteroscedasticity in daily wind speed measurements’, *Theoretical and Applied Climatology* **56**(1-2), 113–122.
- Tomassini, M., Kelly, G. & Saunders, R. (1999), ‘Use and impact of satellite atmospheric motion winds on ecmwf analyses and forecasts’, *Monthly Weather Review* **127**(6), 971–986.
- WeatherOnline (2018), ‘Calima’, <https://www.weatheronline.co.uk/reports/wind/The-Calima.htm>.